



## Helium bubbles enhance strength and ductility in small-volume Al-4Cu alloys

Shi-Hao Li<sup>a</sup>, Jian Zhang<sup>b</sup>, Wei-Zhong Han<sup>a,\*</sup>

<sup>a</sup> Center for Advancing Materials Performance from the Nanoscale (CAMP-Nano), Hysitron Applied Research Center in China (HARCC), State Key Laboratory for Mechanical Behavior of Materials, Xi'an Jiaotong University, Xi'an 710049, PR China

<sup>b</sup> College of Energy, Xiamen University, Xiamen 361005, PR China



### ARTICLE INFO

#### Article history:

Received 10 December 2018

Received in revised form 15 February 2019

Accepted 16 February 2019

Available online xxx

#### Keywords:

Helium bubbles

Al-4Cu

Deformability

Bubble coalescence

*In situ*

### ABSTRACT

By adopting *in situ* nano-mechanical testing in transmission electron microscope, we reveal that nanoscale helium bubbles can simultaneously enhance strength and ductility in small-volume single-crystal Al-4Cu pillars, which breaks the paradox of trade-off between strength and ductility. Nanoscale helium bubbles serve as internal dislocation sources and shearable obstacles, which promote dislocation nucleation and storage, and give rise to higher flow stress, controllable plasticity and larger uniform deformation in Al-4Cu pillars. Nanoscale helium bubbles are rather stable under plastic straining. Bubble coarsening and coalescence are only observed at final localized deformation regime.

© 2019 Acta Materialia Inc. Published by Elsevier Ltd. All rights reserved.

Small-volume materials play an increasing important role in the development of micro- and nano-technology in the past decades [1,2]. Since the dimensions of small-volume materials are comparable to the dislocation mean free path, abundant dislocations tend to glide to the free surface and annihilate quickly during straining, leading to stochastic plasticity, limited uniform deformability and zero strain hardening *etc.* [1–5]. These unfavorable deformation characters plague the mechanical performance of small-volume materials. Various strategies have been proposed to eliminate these unfavorable deformation characters. For example, interfaces [6,7], precipitates [8,9] and artificially deposited thin shell [10,11] were introduced to improve the plasticity of small-volume metals. However, lacking of dislocation storage, frequent strain bursts and limited strain hardening are still identified as unfavorable deformation characters in small-volume metals [6–11]. Therefore, how to achieve the controlled plasticity in small-volume metals still remains a concern.

Tuning dislocation behaviors, such as enhancing dislocation nucleation, reducing dislocation mean free path, promoting dislocation storage are three key aspects to enhance the mechanically properties of small-volume metals [3–11]. Our early work [12,13] demonstrated that the native ultrathin oxide shell in nanoscale Al samples exerts a strong back stress on dislocations during straining, which enhances dislocation storage, and gives rise to the ultrahigh strength and toughness, while the ductility is still limited. In order to further improve

their deformability, it is necessary to introduce other microstructures to further improve dislocation nucleation and dislocation storage. Fortunately, ion beam processing provides a potential mean to realize this goal. Ion beam processing has long been neglected in tuning strength and ductility due to the adverse effects of radiation damage on materials [14,15]. In general, radiation damage leads to hardening and embrittlement of bulk metals [14,15]. For example, helium bubbles, as a typical radiation defects, are always segregating along grain boundaries in irradiated metals, leading to intergranular brittle fracture [14,15]. However, here we reveal that nanoscale helium bubbles can improve deformability of small-volume single-crystal Al alloy pillars. Nanoscale helium bubbles serving as dislocation nucleation sites and shearable obstacles can dramatically enhance dislocation nucleation, reduce dislocation mean free path, promote dislocation storage, and contribute to high flow stress, controllable plasticity and enhanced uniform deformability in small-volume single-crystal Al-4Cu alloy.

We choose peak-aged Al-4Cu alloy as our model material. The Al-4Cu sample is irradiated using 400 keV helium ions at 473 K to a dose of  $2 \times 10^{17}$  ions  $\text{cm}^{-2}$ . As shown in Fig. 1(a), the variation of radiation damage (the red curve, displacement per atom-dpa) and helium concentration (the blue curve, at.%) along depth is estimated using the Stopping and Range of Ions in Matter (SRIM) simulation using full cascade damage mode and an average displacement energy of 25 eV [16]. The helium concentration increases with the increasing of depth, reaching the peak value of about 12 at.% at the depth of about 1.5  $\mu\text{m}$ , and then decreases rapidly. The predicted concentration of helium concentration matches well with helium bubble distribution, as shown in

\* Corresponding author.

E-mail address: [wzhanxjtu@mail.xjtu.edu.cn](mailto:wzhanxjtu@mail.xjtu.edu.cn) (W.-Z. Han).

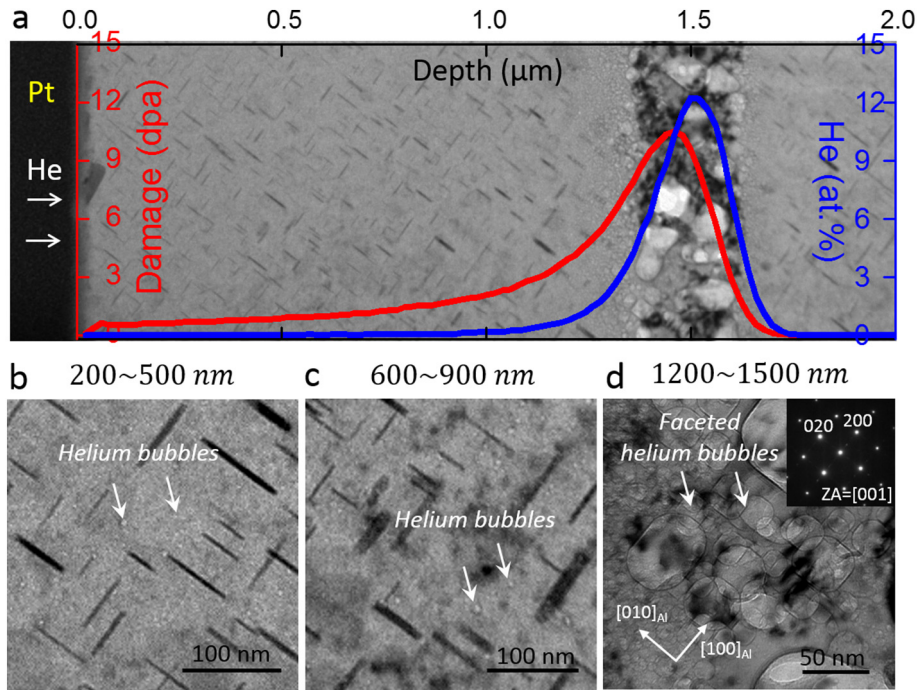


**Fig. 1.** Microstructure of helium irradiated Al-4Cu alloy. (a) The variation of damage and helium concentration along depth; (b)–(d) Morphology of helium bubbles at various locations.

**Fig. 1** (a). The size and density of helium bubbles at different helium concentration were characterized using a transmission electron microscope (JEOL 2100F, TEM). For regions near the free surface, the concentration of helium is pretty low, and small spherical helium bubbles can be observed with under-focused imaging for depth ranging from 200 to 500 nm (**Fig. 1** (b)). With increasing depth, slightly larger and denser bubbles form and distribute homogeneously in the range of 600–900 nm, as shown in **Fig. 1** (c). The concentration of helium increases sharply with further increasing depth. Dense bubbles with diameter of tens of nanometers are formed at the depth ranging from 1200 to 1500 nm. Notably, these large bubbles show facets along {001} matrix plane, which are similar to the faceted bubbles observed in other metals [17]. Three thin samples were lifted out for TEM characterization. All these samples have similar helium bubble distribution and bubble morphologies.

We first conducted *in situ* compressive tests on small-volume single-crystal Al-4Cu pillars with and without helium bubbles. All pillars for compressive tests were fabricated by focused ion beam (FIB) micromachining and tested under displacement control mode using Hysitron PicoIndenter (PI95) in TEM. To obtain pillars containing helium bubbles with proper size and density, all small-volume single-crystal helium-bubbled Al-4Cu pillars were fabricated at the depth of about 600 to 900 nm. The cross-section of the samples for *in situ* testing is  $D \approx 280$  nm. Dense helium bubbles with a diameter of about 4 nm can be observed in this region (**Fig. 1** (c)). **Fig. 2** (a)–(c) show typical compression behaviors of small-volume single-crystal Al-4Cu pillar and helium-bubbled Al-4Cu pillar. The Al-4Cu pillar delivers a yield strength of about 0.48 GPa, followed by a serrated plastic deformation behavior. Large strain bursts are

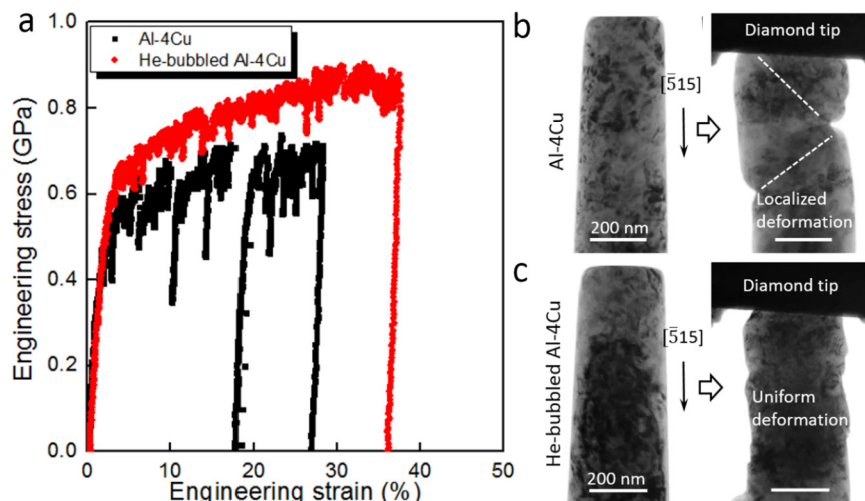


**Fig. 2.** Compressive tests on small-volume single-crystal Al-4Cu with and without helium bubbles. (a) Typical stress-strain curves of Al-4Cu pillars; (b) Deformation morphology of Al-4Cu pillar; (c) Deformation morphology of Al-4Cu pillar with helium bubbles.

frequently observed, as shown in Fig. 2(a) and Movie S1. In addition, localized deformation can be identified, which corresponds to the strain bursts. However, the helium-bubbled Al-4Cu pillar with similar sample dimension and the same loading orientation delivers quite different deformation behavior. The helium-bubbled pillar yields at about 0.58 GPa, followed by a stable and continuous stress-strain response, as shown in Fig. 2(a) and Movie S2. Compared with the bubble-free pillar, the helium-bubbled pillar exhibits higher flow stress and controllable plasticity. Contrary to sharp slip steps observed in the Al-4Cu pillar, the helium-bubbled pillar shows homogeneous plasticity after yielding without obvious localized deformation, as shown in Fig. 2(c). Notably, the Al-4Cu pillar and the helium-bubbled Al-4Cu pillar deliver similar elastic modulus. This indicates that helium bubbles have negligible effects on the elastic properties due to relatively low volume fraction of helium bubbles (Fig. 1(a) and (c)). From the comparison of the Al-4Cu pillar and helium-bubbled Al-4Cu pillar, it is evident that nanoscale helium bubbles play a critical role in promoting dislocation storage, leading to higher flow stress and controllable plasticity in small-volume single-crystal Al-4Cu alloy.

We subsequently performed *in situ* tensile tests on small-volume single-crystal Al-4Cu pillars with and without helium bubbles. To guarantee the same bubble distribution, all helium-bubbled Al-4Cu pillars for tensile tests were fabricated at the same depth as pillars for compressive tests. Tensile tests were conducted under displacement control mode using Hysitron PI95. Fig. 3(a) displays typical true stress-strain curves of both Al-4Cu pillar and helium-bubbled Al-4Cu pillar. As shown in Fig. 3(a) and Movie S3, both the Al-4Cu pillar and the helium-bubbled Al-4Cu pillar deliver stable deformation until localized deformation happens, this agrees well with our previous work [13]. The Al-4Cu pillar with  $[1\bar{1}2]$  orientation yields at about 0.55 GPa (defined as the flow stress at 0.2% plastic strain), followed by a short-time stable uniform deformation stage before localized deformation. As shown in Fig. 3(a), the plastic uniform elongation is 1.6%. Notably, a remarkable stable uniform deformation stage in helium-bubbled pillar can be identified after yielding. The plastic uniform elongation is approximately 2.9%, which is nearly twice of Al-4Cu pillar. Contrary to helium embrittlement caused by bubble/void coalescence in polycrystalline metals [14,15], helium-bubbled single-crystal Al-4Cu pillar delivers higher strength and larger uniform ductility.

To understand the enhanced flow stress and uniform deformability in Al-4Cu pillar containing helium bubbles, we investigate the details of deformation process of a helium-bubbled Al-4Cu pillar with loading direction along  $[2\bar{2}1]$ . Fig. 3(b) shows TEM images extracted from Movie S3 that records the tensile behavior of helium-bubbled Al-4Cu pillar.

High-density of helium bubbles (white dots) distribute homogeneously across the whole pillar. Before straining, the interior of the pillar is roughly clean besides some contrast from dislocations located at the left part of the pillar (Fig. 3(b)-I). With gradually increasing strain, numerous dislocations began to nucleate homogeneously in the sample, as labeled in Fig. 3(b)-II and Movie S3. The strain hardening stage is identified after yielding and the whole pillar delivers stable, continuous and uniform deformation behavior. Notably, instead of typical dislocation avalanche in other small-volume pillars [1–5], dense dislocations nucleate and accumulate continuously and uniformly across the whole sample (as labeled in Fig. 3(b)-II and -III), which prevents localized deformation and gives rise to the enhanced uniform deformability in helium-bubbled Al-4Cu pillar. During the uniform deformation stage, helium bubbles are stable and no obvious bubble coarsening or coalescence happens. With loading proceeds, localized deformation appears after a considerable uniform deformation. Finally, localized deformation is identified at the left part of the pillar. The necking region is getting thinner and thinner with increasing of strain, which provide us an opportunity to investigate bubble evolution processes under straining.

Fig. 4(a)–(e) and Movie S4 reveal helium bubble evolution process under straining in detail. With increasing strain, helium bubbles coarsening is identified and several large helium bubbles form at the necking region, as labeled in Fig. 4(b). These coarsened bubbles are subsequently elongated severely along the loading direction. As shown in Fig. 4(c), spherical bubbles gradually transform into rodlike bubbles with large aspect ratio. Interestingly, further localized deformation split these elongated bubbles into several small bubbles [18,19], as marked in Fig. 4(d). Small bubbles subsequently develop into large bubbles with further straining (Movie S4). Finally, these bubbles coalesce with adjacent bubbles, and cause the final fracture. Our tensile tests indicate that bubble coarsening and coalescence play a critical role in the final fracture of Al-4Cu pillar with helium bubbles.

Our *in situ* mechanical tests demonstrate that small-volume single-crystal helium-bubbled Al-4Cu alloy deliver higher flow stress, controllable plasticity and enhanced uniform deformability. Given the common strength-ductility trade-off in metals [20,21], it seems quite unique that helium bubbles can enhance the strength and ductility of Al-4Cu pillars simultaneously. The role of helium bubbles in plastic deformation can be described as follows. First, compared to the corner/surface of nanopillar, helium bubbles are preferential dislocation nucleation sites [18]. Dislocation emission from the helium bubbles was observed in the bending tests of Cu containing helium bubbles [18]. Simulations show that the activation energy for dislocation nucleation at helium bubbles is lower than that of at the corner/surface of nanopillar, thus a much higher dislocation nucleation frequency at helium bubbles [18].

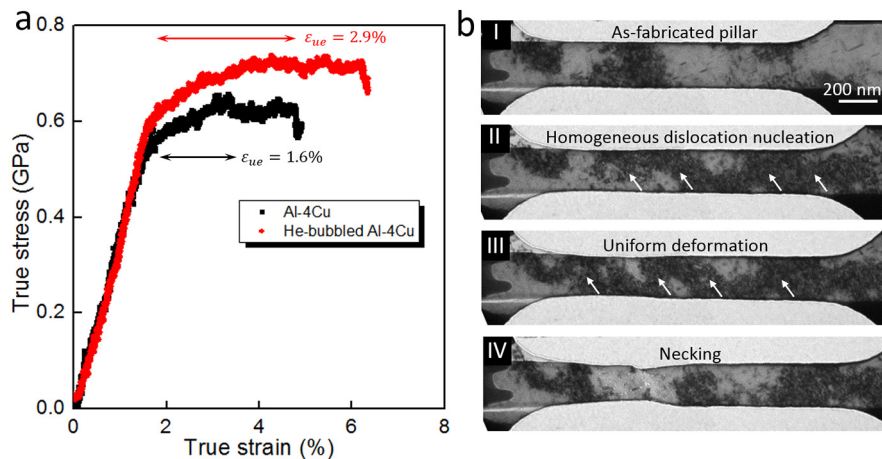
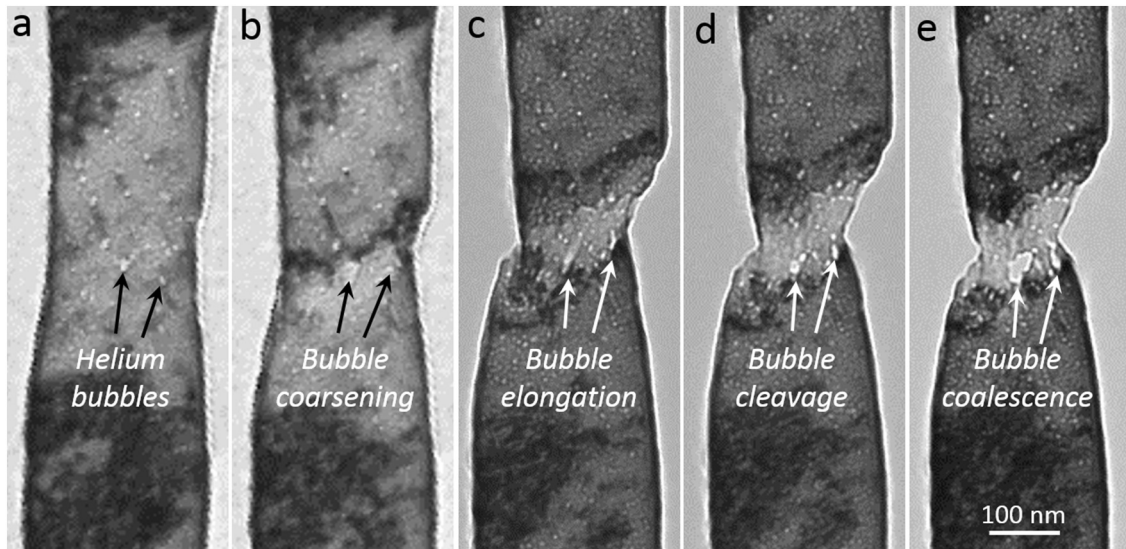


Fig. 3. Tensile tests on small-volume single-crystal Al-4Cu pillars with and without helium bubbles. (a) True stress-strain curves of small-volume Al-4Cu pillars; (b) Strain contrast variation during tensile of Al-4Cu pillars with helium bubbles.



**Fig. 4.** Helium bubble evolution during necking stage. (a) Dense helium bubbles in necking region; (b) Coarsening of helium bubbles with increasing strain; (c) Severe elongation of helium bubbles along loading direction; (d) Cleavage of helium bubble (e) Helium bubble coalescence leads to final fracture.

It is difficult to capture the details of dislocation nucleation during *in situ* straining. However, the near homogenous dislocation activities across the whole sample (Fig. 3(b)-II and Movie S3) indicates that dense and uniform bubbles promote dislocation nucleation, in contrast to the localized deformation in bubble-free Al-4Cu pillars. Second, dense helium bubbles are obstacles for dislocations in metals [22–29]. Dislocations are forced to cut through dense bubbles to carry plastic strain, leading to notable strain hardening and controllable plasticity. Although bubble coarsening and coalescence lead to the final fracture, the role of helium bubbles here is quite different from the bubbles in grain boundaries [30]. As mentioned above [14,15], bubble coarsening and coalescence are easily activated along grain boundaries in polycrystalline metals, which promote crack nucleation and intergranular fracture. However, bubbles in single-crystal Al-4Cu pillars are quite stable under straining (Fig. 3(b) and Movie S3). Bubble coarsening and coalescence are only observed at the final necking stage (Fig. 4 and Movie S4). In general, helium bubbles in Al-4Cu pillars are shearable obstacles due to their low internal pressure (about 1.3 GPa). The internal pressure of equilibrium helium bubbles can be estimated as  $P_{bubble} = 4\gamma_s/d$  [18], where  $\gamma_s$  ( $\sim 1.3$  J/m<sup>2</sup>) is the surface energy of Al [31], and  $d$  ( $\sim 4$  nm) is the diameter of helium bubbles.

Several studies have estimated the hardening induced by helium bubbles in metals [22–28]. Bubble size, density, spacing and internal pressure are critical factors to determine the magnitude of hardening. Lucas [25] proposed that the obstacle strength parameter  $\alpha$  can be adopted to describe the interactions between dislocations and obstacles in various metals. Generally, the obstacle strength  $\alpha$  ranges from 0 to 1. The obstacles are shear-resistant (strong obstacles) for  $\alpha = 1$  and dislocations are forced to bow out and then bypass these obstacles. The corresponding hardening induced by dislocations and obstacles interactions can be evaluated using Orowan model [32]. Shearable obstacles (weak obstacles) have  $\alpha < 1$ , which means shearable obstacles have weaker hardening effect [24,25]. Instead of bypassing these obstacles, dislocations can cut through shearable obstacles at elevated shear stress. The value of obstacle strength parameter for helium bubble can be determined by [27]

$$\alpha = \frac{\Delta\tau l}{\mu b} \quad (1)$$

where  $\Delta\tau$  is the net increase of shear strength by helium bubbles,  $l$  is the average spacing of bubbles ( $\sim 30.5$  nm),  $\mu$  is the shear modulus,  $b$  is the

Burgers vector. We obtain a value of  $\alpha = 0.18$  for compressive tests and  $\alpha = 0.15$  for tensile tests in Al-4Cu pillar containing helium bubbles, which is comparable to 0.2 proposed in Lucas's work [25]. The variation of obstacle strength parameter value in tension and compression is attributed to slightly different in the net increase of shear stress. Therefore, the helium bubbles with low internal pressure can be regarded as weak obstacles with low obstacle strength [24,25].

The strengthening induced by helium bubbles can be evaluated using modified Orowan model [23,24]

$$\Delta\tau = \frac{\mu b}{2\pi l} \ln\left(\frac{l}{rcos\varphi}\right) (cos\varphi)^{3/2} \quad (2)$$

where  $\mu$ ,  $b$  and  $l$  have the same meaning as in Eq. (1),  $r$  is the radius of helium bubbles ( $\sim 2$  nm),  $\varphi$  is defined as half of the critical angle of a bow-out dislocation and equals to  $\sim 60^\circ$  for helium bubbles in Al-4Cu pillars [24]. The estimated strengthening by helium bubbles is about 48 MPa. Taking the yield strength of Al-4Cu pillars as a reference, the net increase of shear stress is 45 MPa for compressive tests and 36 MPa for tensile tests, respectively. Therefore, our experimental data in general agree well with the estimation calculated using the modified Orowan model.

In summary, dense nanoscale helium bubbles are formed in Al-4Cu alloy after helium implantation. Helium implanted small-volume Al-4Cu single-crystal pillars deliver higher flow stress, controllable plasticity and larger uniform deformability than the full dense Al-4Cu pillar. Similar to the helium bubbles in Cu, dense bubbles in Al-4Cu alloy also play a role of active internal dislocation sources and shearable obstacles, which promote homogeneous dislocation nucleation and storage across the whole sample. Helium bubbles are rather stable during uniform deformation stage. Localized deformation dramatically accelerates bubble coarsening and coalescence, leading to the final fracture of samples.

Supplementary data to this article can be found online at <https://doi.org/10.1016/j.scriptamat.2019.02.025>.

#### Acknowledgements

This work was supported by the National Key Research and Development Program of China (2017YFB0702301) and the National Natural Science Foundation of China (Grant Nos. 51471128, 51621063), the 111 Project of China (Grant No. BP2018008) and the Innovation Project of Shaanxi Province (Grant No. 2017KTPT-12).

**References**

- [1] M.D. Uchic, D.M. Dimiduk, J.N. Florando, W.D. Nix, *Science* 305 (2004) 986–990.
- [2] T. Zhu, J. Li, *Prog. Mater. Sci.* 55 (2010) 710–757.
- [3] S.H. Oh, M. Legros, D. Kiene, G. Dehm, *Nat. Mater.* 8 (2009) 95–100.
- [4] F. Momprou, M. Legros, A. Sedlmayr, D.S. Gianola, D. Cailard, O. Kraft, *Acta Mater.* 60 (2012) 977–983.
- [5] H. Bei, S. Shim, S.M. Pharr, E.P. George, *Acta Mater.* 56 (2008) 4762–4770.
- [6] A. Kunz, S. Pathak, J.R. Greer, *Acta Mater.* 59 (2011) 4416–4424.
- [7] D.C. Jang, C. Cai, J.R. Greer, *Nano Lett.* 11 (2011) 1743–1746.
- [8] R. Gu, A.H.W. Ngan, *Scr. Mater.* 68 (2013) 861–864.
- [9] B. Girault, A.S. Schneider, C.P. Frick, E. Arzt, *Adv. Eng. Mater.* 12 (2010) 385–388.
- [10] K.S. Ng, A.H.W. Ngan, *Acta Mater.* 57 (2009) 4902–4910.
- [11] A.T. Jennings, C. Gross, F. Greer, Z.H. Aitken, S.-W. Lee, C.R. Weinberger, J.R. Greer, *Acta Mater.* 60 (2012) 3444–3455.
- [12] S.H. Li, W.Z. Han, Z.W. Shan, *Acta Mater.* 141 (2017) 183–192.
- [13] S.H. Li, W.Z. Han, J. Li, E. Ma, Z.W. Shan, *Acta Mater.* 126 (2017) 202–209.
- [14] H. Schroeder, P. Batfalsky, *J. Nucl. Mater.* 117 (1983) 287–294.
- [15] H. Trinkaus, H. Ullmaier, *J. Nucl. Mater.* 212–215 (1994) 303–309.
- [16] J.F. Ziegler, M.D. Ziezler, J.P. Biersack, *Nucl. Inst. Methods Phys. Res. B* 268 (2010) 1818–1823.
- [17] Q.M. Wei, N. Li, K. Sun, L.M. Wang, *Scr. Mater.* 63 (2010) 430–433.
- [18] M.S. Ding, J.P. Du, L. Wan, S. Ogata, L. Tian, E. Ma, W.Z. Han, J. Li, Z.W. Shan, *Nano Lett.* 16 (2016) 4118–4124.
- [19] M.S. Ding, L. Tian, W.Z. Han, J. Li, E. Ma, Z.W. Shan, *Phys. Rev. Lett.* 117 (2016) 215501.
- [20] E. Ma, T. Zhu, *Mater. Today* 20 (2017) 323–331.
- [21] I.A. Ovid'ko, R.Z. Valiev, Y.Z. Zhu, *Prog. Mater. Sci.* 94 (2018) 462–540.
- [22] A. Reichardt, M. Ionescu, J. Davis, L. Edwards, R.P. Harrison, P. Hosemann, D. Bhattacharyya, *Acta Mater.* 100 (2015) 147–154.
- [23] N. Li, M. Nastasi, A. Misra, *Int. J. Plast.* 32–33 (2012) 1–16.
- [24] Q.M. Wei, N. Li, N. Mara, M. Nastasi, A. Misra, *Acta Mater.* 59 (2011) 6331–6340.
- [25] G.E. Lucas, *J. Nucl. Mater.* 206 (1993) 287–305.
- [26] N. Li, M. Demkowicz, N. Mara, Y.Q. Wang, A. Misra, *Mater. Res. Lett.* 4 (2016) 75–82.
- [27] Z.J. Wang, F.I. Allen, Z.W. Shan, P. Hosemann, *Acta Mater.* 121 (2016) 78–84.
- [28] Q. Guo, P. Landau, P. Hosemann, Y.Q. Wang, J.R. Greer, *Small* 9 (2013) 691–696.
- [29] W.Z. Han, M.S. Ding, R.L. Narayana, Z.W. Shan, *Adv. Eng. Mater.* 19 (2017) 1700357.
- [30] W.Z. Han, M.S. Ding, Z.W. Shan, *Scr. Mater.* 147 (2018) 1–5.
- [31] L. Vitos, A.V. Ruban, H.L. Skriver, J. Kollar, *Surf. Sci.* 411 (1998) 186–202.
- [32] J.C. Teixeira, D.G. Cram, L. Bourgeois, T.J. Bastow, A.J. Hill, C.R. Hutchinson, *Acta Mater.* 56 (2008) 6109–6122.